Received: 7 January 2023 | Revised: 10 February 2023 | Accepted: 10 February 2023

DOI: 10.1002/agt2.330

Aggregate WILEY

REVIEW

An overview on AIEgen-decorated porphyrins: Current status and applications

Govardhana Babu Bodedla[1,2,3] | **Xunjin Zhu**[3] | **Wai-Yeung Wong**[1,2]

[1]Department of Applied Biology & Chemical Technology and Research Institute for Smart Energy, The Hong Kong Polytechnic University, Hong Kong, P. R. China

[2]The Hong Kong Polytechnic University Shenzhen Research Institute, Shenzhen, P. R. China

[3]Department of Chemistry, Hong Kong Baptist University, Hong Kong, P. R. China

Correspondence
Govardhana Babu Bodedla, Department of Applied Biology & Chemical Technology and Research Institute for Smart Energy, The Hong Kong Polytechnic University, Hong Kong, P. R. China.
Email: govardhan.bodedla@gmail.com

Xunjin Zhu, Department of Chemistry, Hong Kong Baptist University, Waterloo Road, Kowloon Tong, Hong Kong, P. R. China.
Email: xjzhu@hkbu.edu.hk

Wai-Yeung Wong, Department of Applied Biology & Chemical Technology and Research Institute for Smart Energy, The Hong Kong Polytechnic University, Hong Kong, P. R. China.
Email: wai-yeung.wong@polyu.edu.hk

Funding information
Science, Technology and Innovation Committee of Shenzhen Municipality, Grant/Award Number: JCYJ20180507183413211; RGC Senior Research Fellowship Scheme, Grant/Award Number: SRFS2021-5S01; National Natural Science Foundation of China, Grant/Award Number: 52073242; Hong Kong Polytechnic University; General Research Fund, Grant/Award Number: 12304320; Hong Kong Research Grants Council

Abstract

One of the major obstacles of porphyrins is the aggregation-caused quenching (ACQ) of photoluminescence due to the strong intermolecular π–π interaction of the planar porphyrin core in the solid state. However, ACQ leads to the nonradiative deactivation of the photoexcited states which results in short-lived charge-separated states and thus low photoluminescence and singlet quantum yields. This phenomenon would limit the utilization of porphyrins in near-infrared fluorescent bioimaging, photodynamic therapy, photocatalytic hydrogen evolution, electrochemiluminescence, and chiroptical applications. Hence, to address the ACQ property of porphyrins and enhance the performance of the above applications, a limited number of AIEgen-decorated porphyrins have been designed, synthesized, and tested for their applications. It has been found that the introduction of AIEgens, such as tetraphenylethylene, diphenylacrylonitrile, (3,6-bis-(1-methyl-4-vinylpyridinium)-carbazole diiodide, and iridium motif into the porphyrin core, transformed the porphyrins from ACQ to aggregation-induced emission (AIE) in their solid state due to the reduced strong intermolecular π–π stacking of porphyrins. Consequently, such porphyrins containing AIE features are employed as potential candidates in the above-mentioned applications. In this review, we summarize the AIEgen-decorated porphyrins which have been published to date, and also discuss the benefits of converting porphyrins from ACQ to AIE for enhanced performance within each application. As far as we know, there is no review that summarizes the structures and applications of AIEgen-decorated porphyrins to date. Therefore, we presume that this review would be helpful to design more efficient AIEgen-decorated porphyrins for a wide range of applications in the future.

KEYWORDS

aggregation-caused quenching, aggregation-induced emission, AIE luminogen, FRET and solid state emission, porphyrin

Abbreviations: $^1O_2$, singlet oxygen; ACN, acetonitrile; ACQ, aggregation-caused quenching; AIE, aggregation-induced emission; AIECL, aggregation-induced electrochemiluminescence; BMVC, (3,6-bis-(1-methyl-4-vinylpyridinium)-carbazole diiodide; CD, circular dichroism; $CHCl_3$, chloroform; CPL, circularly polarized luminescence; DAN, diphenylacrylonitrile; DFT, density functional theory; DHPA, *N*,*N*′-di-(2,3-dihydroxypropyl)-9,10-anthracenedipropanamide; DLS, dynamic light scattering; DMF, dimethylformamide; DPP, diphenylphenanthrene; DPBF, 1,3-diphenylisobenzofuran;; DSPE-PEG, 1,2-distearoyl-sn-glycero-3-phosphoethanolamine-*N*-[methoxy (polyethylene glycol)]; ECL, electrochemiluminescence; FONs, fluorescent organic nanoparticles; FRET, Förster resonance energy transfer; f_w, H_2O fraction; H_2O, water; HOMO, highest occupied molecular orbital; ICT, intramolecular charge-transfer; IET, intramolecular energy transfer; Ir-motif, iridium motif; $K_2S_2O_8$, potassium persulfate; KCl, potassium chloride; Lop P, lipophilicity; LUMO, lowest unoccupied molecular orbital; MeOH, methanol; MTT, 3-(4,5-dimethylthiazol-2-yl)-2,5-diphenyltetrazolium bromide; NIR, near-infrared; NPs, nanoparticles; OLEDs, organic light emitting diodes; PBS, phosphate-buffered saline; PDT, photodynamic therapy; PHE, photocatalytic hydrogen evolution; ROSs, reactive oxygen species; SEM, scanning electron microscopy; TEM, transmission electron microscopy; THF, tetrahydrofuran; TICT, twisted intermolecular charge transfer; TAPs, tetraazaporphyrins; TPE, tetraphenylethylene; Zn, zinc; ZnPc, zinc phthalocyanine; ε, molar extinction coefficient; Φ_Δ, singlet oxygen quantum yield; Φ_{PL}, photoluminescence quantum yield.

1 | INTRODUCTION

Porphyrin and its derivatives are called a "color of life" due to their extensive availability in the form of natural pigments, such as chlorophyll, protoheme, and vitamin B_{12}. Nevertheless, recently, they have gained much attention in a wide range of applications, such as photovoltaics,[1–4] biomedical fields,[5–8] photocatalytic hydrogen evolution (PHE)[9–14] and carbon dioxide reduction,[15–17] chemical sensors,[18–21] supramolecular chemistry,[22] and organic geochemistry[23,24] because of their excellent light-harvesting ability, visible-to-near-infrared emission, versatile redox properties, and chemical and photochemical stabilities. Besides, the photophysical and electrochemical properties of porphyrins can be facilely modified by linking different chromophores at the four *meso*- and eight β-positions, and the inclusion of variable metals within the porphyrin macrocycle. However, most of the conventional porphyrins tend to form aggregates in the solid state due to strong intermolecular π–π interactions between planar porphyrin cores. Also, hydrogen bonding, electrostatic interactions, van der Waals interactions, and hydrophobic effects can further strengthen the aggregation of porphyrin rings. This phenomenon can trigger the nonradiative deactivation of the photoexcited states and then short-lived charge-separated states, and hence, low photoluminescence quantum yield (Φ_{PL}) and reduced formation of reactive oxygen species (ROSs) due to the photoluminescence quenching/aggregation-caused quenching (ACQ).

So far, some strategies have been developed to disrupt the aggregation of porphyrins by isolating porphyrin molecules in the solid state: (1) the encapsulation of porphyrins with inorganic/organic matrix to form nanostructures;[25–28] (2) a covalent conjugation of dendritic arms to the porphyrin core;[29,30] and (3) introducing bulky groups into the porphyrin macrocycle.[31–35] Though these tactics could prevent the π–π stacking of porphyrin cores in the solid state, the complicated synthesis of such kind of porphyrins and their unstable nanostructures were the major problems. To solve this problem more effectively, the porphyrins were further modified with nonplanar propeller-shaped motifs, namely, tetraphenylethylene (TPE), diphenylphenanthrene (DPP), diphenylacrylonitrile (DAN), (3,6-bis-(1-methyl-4-vinylpyridinium)-carbazole diiodide (BMVC), and iridium motif (Ir-motif) (Figure 1) with aggregation-induced emission (AIE) behavior. It has been found that the introduction of AIE luminogens simply called AIEgens to the porphyrin core is a versatile method to enhance the photoluminescence in the aggregate state and consequently stabilize the photoexcited states (Figure 2). Generally, AIEgens are not emissive in the solution because the free-rotation of phenyl groups deactivates the photoluminescence intensity, whereas such AIEgens can increase the photoluminescence intensity drastically in the solid state owing to the restriction of intramolecular motion. Thus, over the last two decades, many papers have been published based on the AIEgen containing materials for solar cells,[36–38] organic light emitting diodes (OLEDs),[39–42] sensing applications,[43–47] photocatalysis,[48] and biomedical fields.[49–51] On the contrary, very limited papers were published based on the AIEgen-decorated porphyrins for fluorescence bioimaging, photodynamic therapy (PDT), photocatalytic hydrogen evolution (PHE), solid state photoluminescence, electrochemiluminescence (ECL), and self-assembled studies. Herein, we have summarized the AIEgen-decorated porphyrins reported in the literature so far and discussed their AIE properties to further design more efficient porphyrins with AIE properties for wide applications.

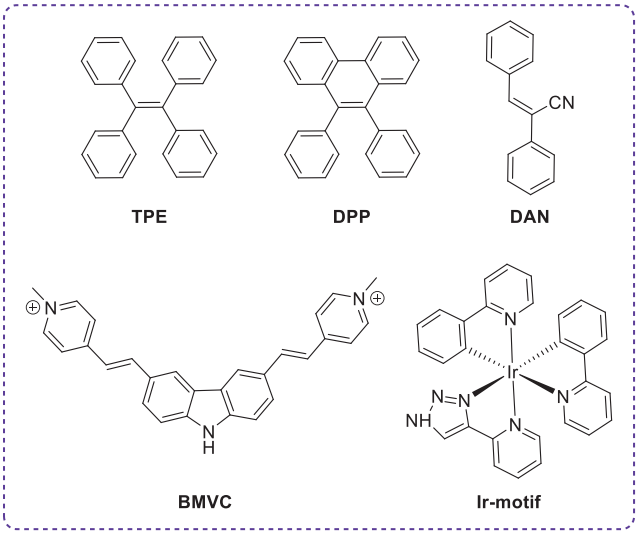

FIGURE 1 Structures of AIEgens attached to porphyrin macrocycle

2 | DISCUSSION

2.1 | Near-infrared (NIR) fluorescence bioimaging

Recently, NIR fluorescent dyes have received much interest for bioimaging applications, such as fluorescence detection of tumors and image-guided surgery owing to their large Stokes shift values, strong fluorescence imaging in dark-field, high tissue penetration, and low biotoxicity.[53,54] Although many porphyrins show intrinsic NIR emissions, the strong ACQ of porphyrins prohibits their applications in NIR fluorescence bioimaging. In order to reduce the ACQ and improve the NIR fluorescence bioimaging in the solid state, a few AIEgen-decorated porphyrins were designed and the corresponding structures are shown in Figure 3.

To convert ACQ porphyrins to become AIE active, Guo et al. have developed a dimethylamino-TPE decorated porphyrin, **1**.[55] This porphyrin shows red-shifted absorption and emission peaks when compared to those of porphyrin **2** without dimethylamino-TPE groups. This could be rationalized by the strong electron-donating property of dimethylamine-TPE motifs compared to that of methyl groups. In tetrahydrofuran (THF)/water (H_2O) mixture, when the H_2O fraction (f_w) was increased, both porphyrins showed red-shifted and broadened absorption peaks with significantly decreased ε, indicating the formation of strong-aggregates in the solid state (Figure 4A,B). It should be noticed that the decreased emission intensity of **2** with the increasing f_w from 0% to 99% is indicative of ACQ, whereas in the case of **1**, initially, the emission intensity decreased from 0% to >30% of f_w due to the twisted intermolecular charge transfer (TICT) resulted from the increased solvent

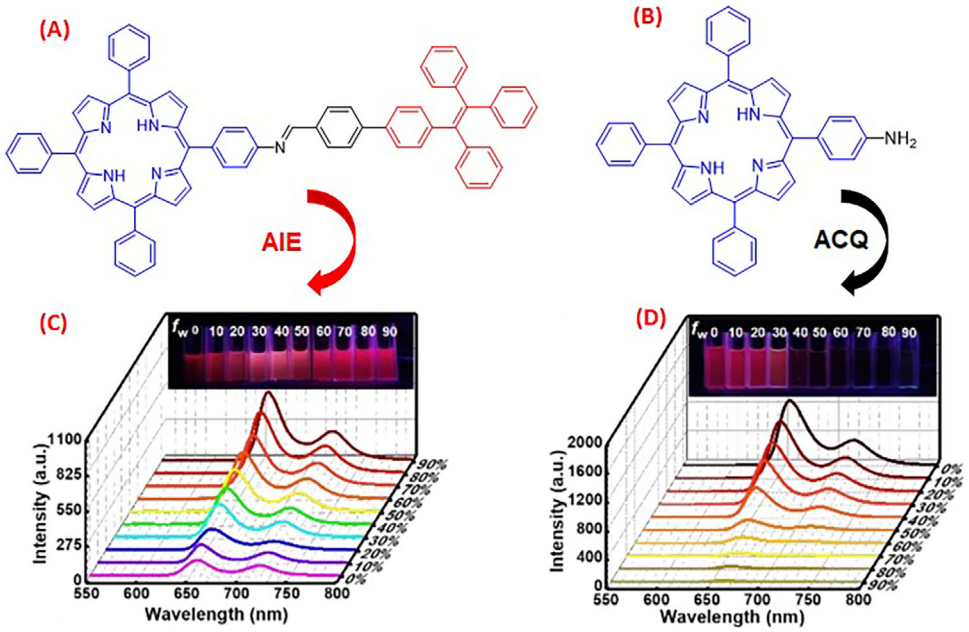

FIGURE 2 (A) Porphyrin with AIEgen. (B) Porphyrin without AIEgen. (C) AIE property of porphyrin with AIEgen. (D) ACQ property of porphyrin without AIEgen. Parts (A–D): Reproduced with permission.[52] Copyright 2020, Wiley-VCH GmbH

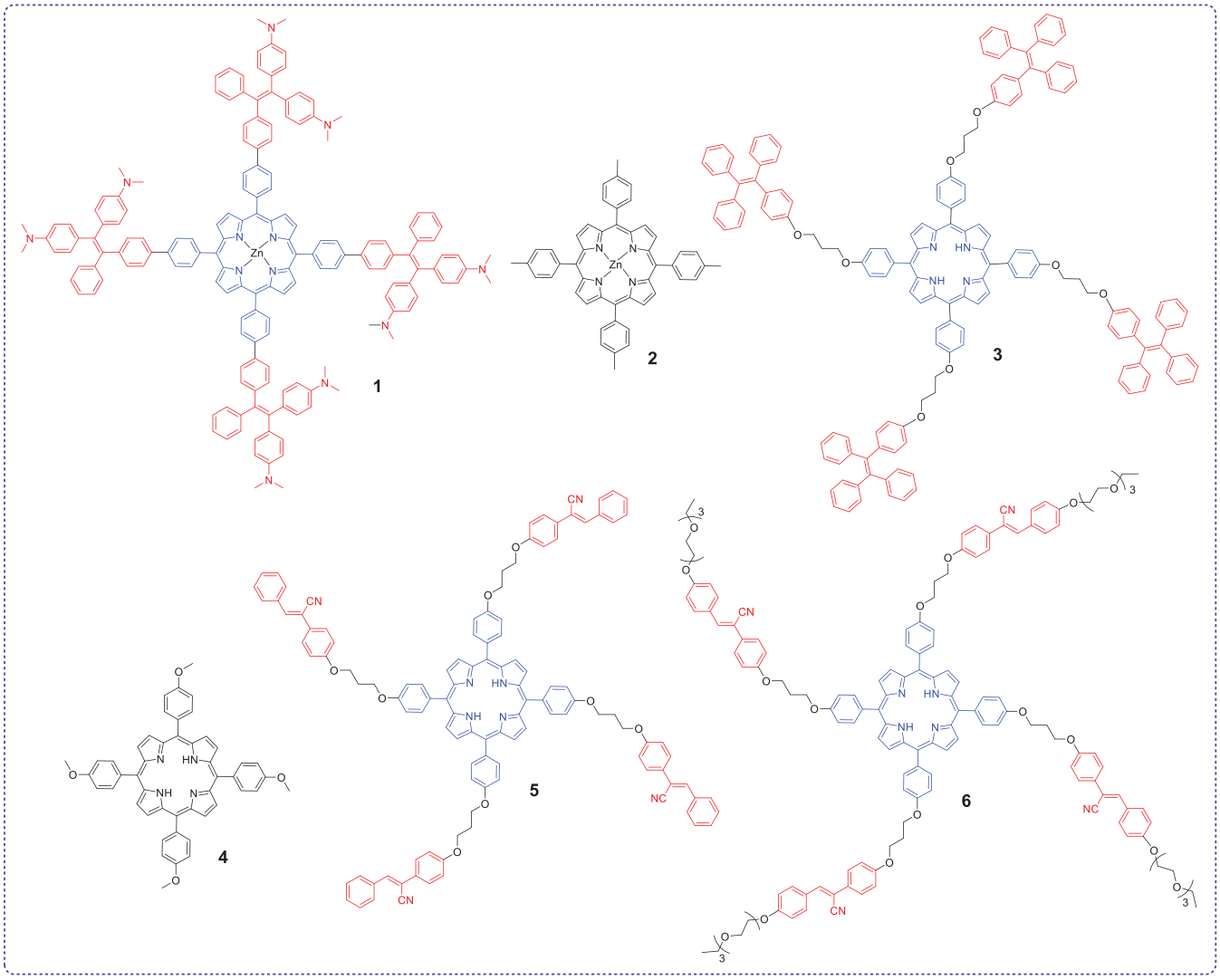

FIGURE 3 Structures of AIEgen-decorated porphyrins and related controlled porphyrins used in the fluorescence bioimaging

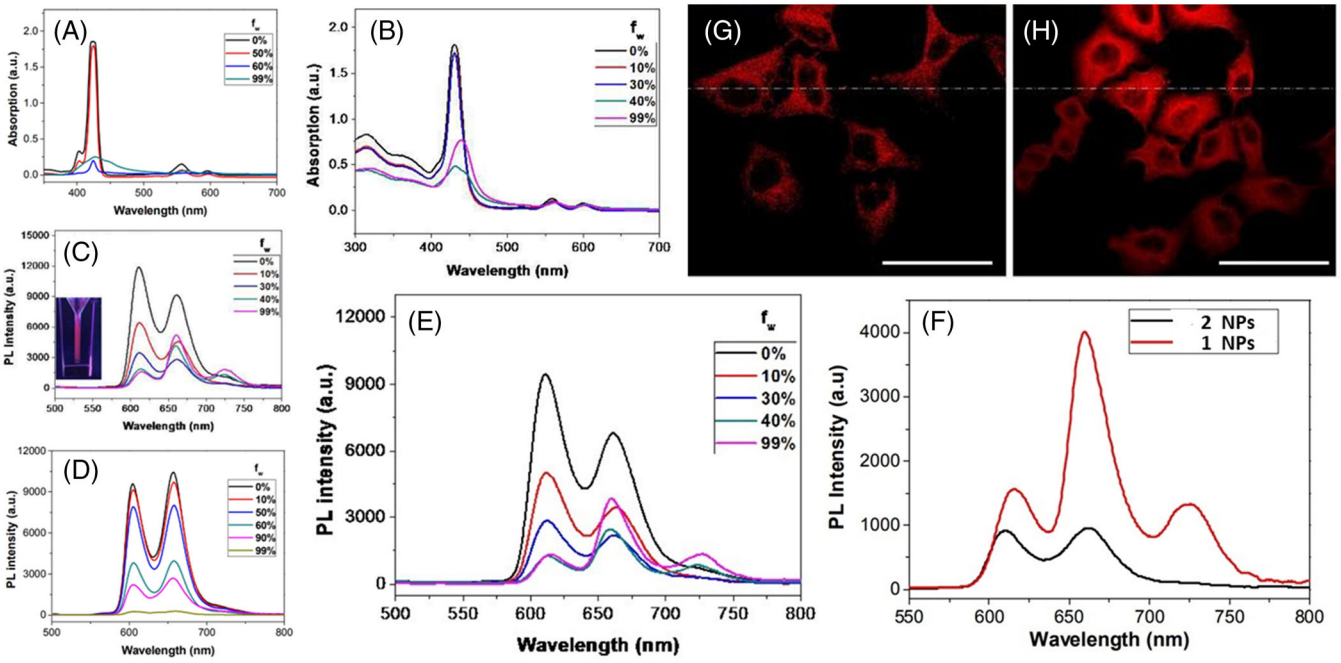

FIGURE 4 Absorption spectra of (A) **2** [10 μM] and (B) **1** [10 μM] in THF/H_2O mixture with different f_w. Emission spectra of (C) **1** [10 μM] and (D) **2** [10 μM] in THF/H_2O mixture with different f_w (λ_{ex} = 410 nm). (E) Emission spectra of **1** [10 μM] in THF/H_2O mixture with different f_w (λ_{ex} = 315 nm). (F) Emission spectra of **1** and **2** NPs [10 μM] in H_2O at room temperature (λ_{ex} = 315 nm). Confocal images of fixed HeLa cells after incubation with (G) 2 μM **2**-derived NPs and (H) 2 μM **1**-derived NPs; scale bar: 50 μm. Parts (A–G): Reproduced with permission.[55] Copyright 2016, Royal Society of Chemistry

polarity and the emission intensity substantially increased when f_w > 40% with a new TICT peak at 725 nm attributed to the AIE effect (Figure 4C,E). Considering the AIE effect and large Stokes shift value of **1** (171 nm) at f_w = 99%, **1** can act as a decent candidate for bioimaging application. More noteworthily, the absence of the emission peak at 551 nm which belongs to the dimethylamine-TPE entities upon excitation at 315 nm is indicative of an intramolecular energy transfer (IET) from the dimethylamino-TPE groups to the porphyrin core (Figure 4E). Nanoparticles (NPs) of **1**/**2** were prepared by adding THF solutions of **1**/**2** and 1,2-distearoyl-sn-glycero-3-phosphoethanolamine-*N*-[methoxy (polyethylene glycol)] (DSPE-PEG) into H_2O. NPs of **1** exhibited a four-fold higher photoluminescence intensity than that of **2** NPs (Figure 4F). By employing **1**-derived NPs for in vitro cellular imaging application, the **1** NPs in HeLa cells showed significantly superior brightness in comparison to that of **2** NPs (Figure 4G,H). These conclusions indicate that the decoration of TPE chromophores to the porphyrin core in **1** is a remarkable approach for attaining excellent bioimaging performance due to the AIE nature.

In another report, porphyrin **3** containing a flexible chain between the TPE groups and the porphyrin ring was synthesized in a satisfactory yield by Yu et al.[56] This porphyrin also possessed an efficient IET between the TPE groups and the porphyrin ring due to the overlapped Soret-band absorption peak of the typical porphyrin macrocycle and emission peak of TPE motifs. Moreover, **3** showed excellent AIE in THF/H_2O mixture as evidenced by gradually increased porphyrin emission peaks at 640–760 nm when increasing the f_w from 0% to 90% (Figure 5A). Due to the combined IET and AIE, porphyrin **3** not only showed bright photoluminescence in the solution but also in the solid state, corresponding to a Φ_{PL} of 0.14. This value is much higher than the controlled porphyrin **4** containing no AIE groups and those AIEgen-decorated porphyrins reported in the literature so far (Figure 5B). More notably, this is the first AIEgen-decorated porphyrin that shows stronger photoluminescence in the solid state. Density functional theory (DFT) calculations revealed that the IET would be Förster resonance energy transfer (FRET) in **3** due to a suitable distance (18.1 Å) between the TPE groups and the porphyrin moiety. Additionally, **3** exhibited a large Stokes shift value of 410 nm between the absorption and the photoluminescence peaks, suggesting a possibility to use it in fluorescence bioimaging behavior for living cells. Since **3** possessed strong emission in the solid state, it was employed in fluorescence bioimaging experiment for in vitro HeLa cells with the support of a fluorescent inverted microscope. The cell viabilities were found to be higher than 80% in the concentration range of 0–40 μM in 24 h, implying a low biotoxicity of **3**. This result suggests the suitability of **3** in NIR fluorescence bioimaging for living cells. Finally, this work also demonstrates that the introduction of soft spacers between the TPE units and the porphyrin core is an efficient strategy for designing strong solid state photoluminescent porphyrin derivatives through AIE-FRET processes.

The same group likewise synthesized porphyrin **5** by introducing four DAN units into the porphyrin skeleton through a soft linker and studied its AIE-FRET property and NIR fluorescence bioimaging application.[57] When compared with the controlled porphyrin **4**, porphyrin **5** showed no obvious change in the absorption pattern except for the appearance of new peaks at 300–360 nm which corresponds to the absorption of DAN units. Emission spectra revealed that both porphyrins have shown a strong ACQ effect for the porphyrin emission peaks at 640 and 760 nm in the THF/H_2O mixture under the excitation of 420 nm that belongs to the porphyrin Soret-band (Figure 5D). However, when the porphyrin **5** was excited at 330 nm which is related to DAN absorption, the

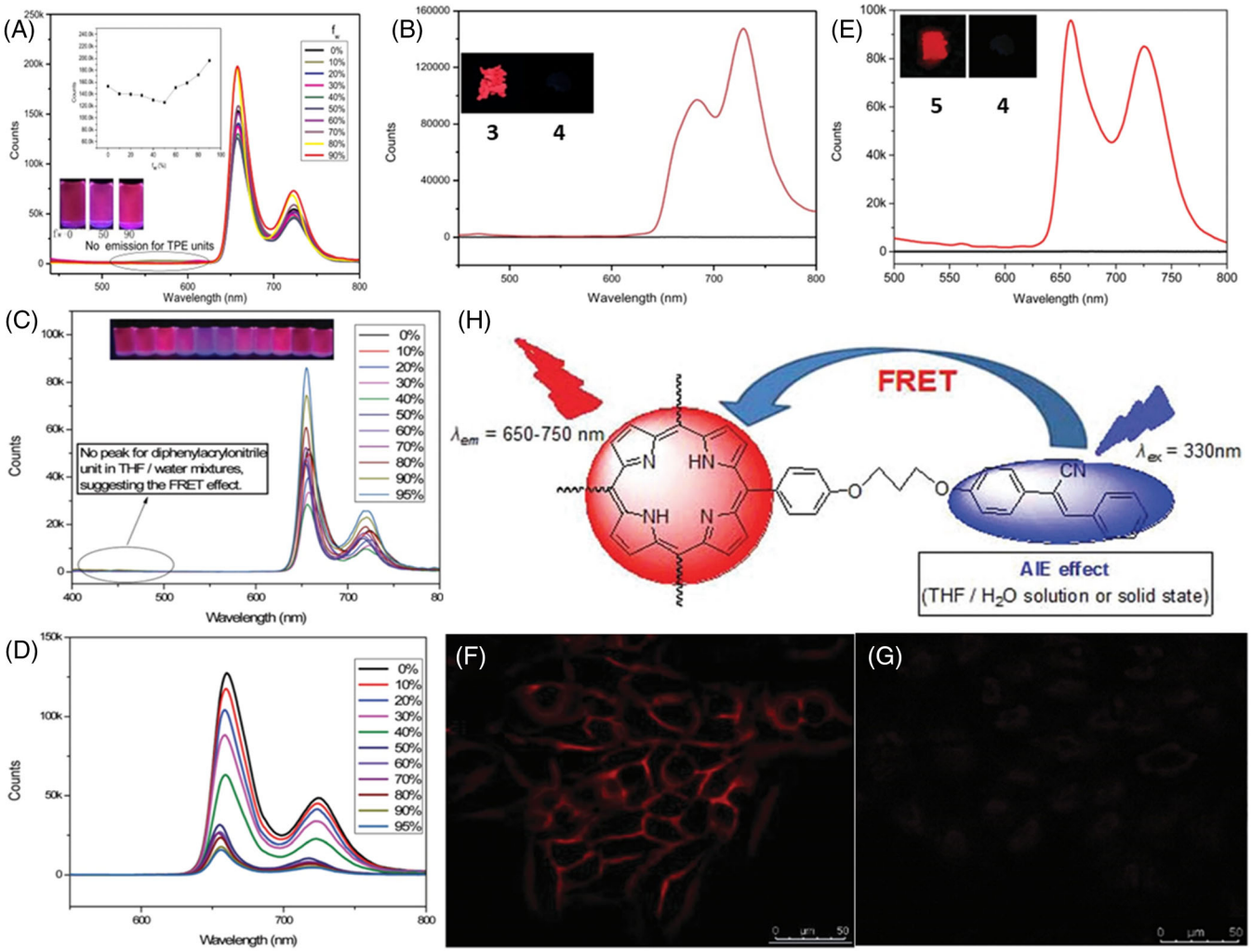

FIGURE 5 (A) Emission spectra of **3** [1 μM] in THF/H_2O mixture with different f_w (λ_{ex} = 320 nm). (B) Emission spectra of **3** (red line) and **4** (black line) in solid state (λ_{ex} = 320 nm); inset photos show fluorescence of **3** and **4**. (C) Emission spectra of **5** [1 μM] in THF/H_2O mixture with different f_w (λ_{ex} = 330 nm). (D) Emission spectra of **5** [1 μM] in THF/H_2O mixture with different f_w (λ_{ex} = 420 nm). (E) Emission spectra of **5** (red line) and **4** (black line) in solid state (λ_{ex} = 330 nm); inset depicts the fluorescence of **5** and **4**. Dark-field images of fluorescence imaging in vitro HeLa cells after incubation with (F) 2 mM of **5** and (G) 2 mM of **4**; scale bar: 50 mm (λ_{ex} = 460–550 nm). (H) Schematic illustration of the AIE-FRET process for **5**. Parts (A,B): Reproduced with permission.[56] Copyright 2020, Elsevier SD. Parts (C–H): Reproduced with permission.[57] Copyright 2019, Royal Society of Chemistry

emission intensity decreased with the increasing f_w from 0% to 40%, and then increased with the increasing f_w from 40% to 95% (Figure 5C). It indicates that there is a fine balance between ACQ and AIE for **5** in THF/H_2O mixture. Besides, the emission peak between 400 and 500 nm belonging to DAN was not observed in THF/H_2O mixture, suggesting an obvious FRET process between the DAN units and the porphyrin ring. Overall, the combined AIE-FRET processes dominate the ACQ when the f_w increases from 40% to 95% in THF/H_2O mixture. All these outcomes advised that the conjugation of DAN units to the porphyrin skeleton suppressed the ACQ and enhanced the emission of porphyrins in the aggregated state. Both porphyrins **4** and **5** showed very weak emission in the solid state under the excitation at 420 nm, while a bright emission was observed for **5** when excited at 330 nm (Figure 5E). It also indicates that the combined AIE-FRET effect plays a major role to produce a strong emission for **5** in the solid state (Figure 5H). Later on, **4** and **5** were investigated for fluorescence imaging in vitro HeLa cells utilizing a fluorescence inverted microscope. It was observed that no fluorescence imaging was observed for sample **4** in the dark field, while a strong red fluorescence imaging was noticed for **5** (Figure 5F,G). Moreover, porphyrin **5** in cells delivered more intense red luminescence in comparison to that of **4**. Also, at a concentration of 2 mM, the cell viabilities of 90% and 86% for 12 and 24 h, respectively, were observed for HeLa cell metabolic activity of **5** containing 3-(4,5-dimethylthiazol-2-yl)-2,5-diphenyltetrazolium bromide (MTT) assay. This result denotes the excellent NIR fluorescence bioimaging capability of **5** possessing AIE-FRET property.

Porphyrin **6** was developed by attaching polyglycol chains to the DAN moiety of porphyrin **5**.[58] Porphyrin **6** shows a FRET between the DAN moieties and the porphyrin ring due to the overlapped emission peak of DAN groups and the Soret-band absorption peak of the porphyrin macrocycle. Similarly, this porphyrin in THF/H_2O mixture also showed ACQ when excited at 420 nm which belongs to the porphyrin core, whereas under the excitation of 330 nm corresponding to DAN exhibited AIE (Figure 6A,B). The AIE nature of porphyrin **6** could be ascribed to the AIEgen DAN which effectively suppressed the nonradiative decay channels of porphyrin moiety due to the strong FRET. Porphyrin **6** displayed well-ordered hexagonal columnar mesophase

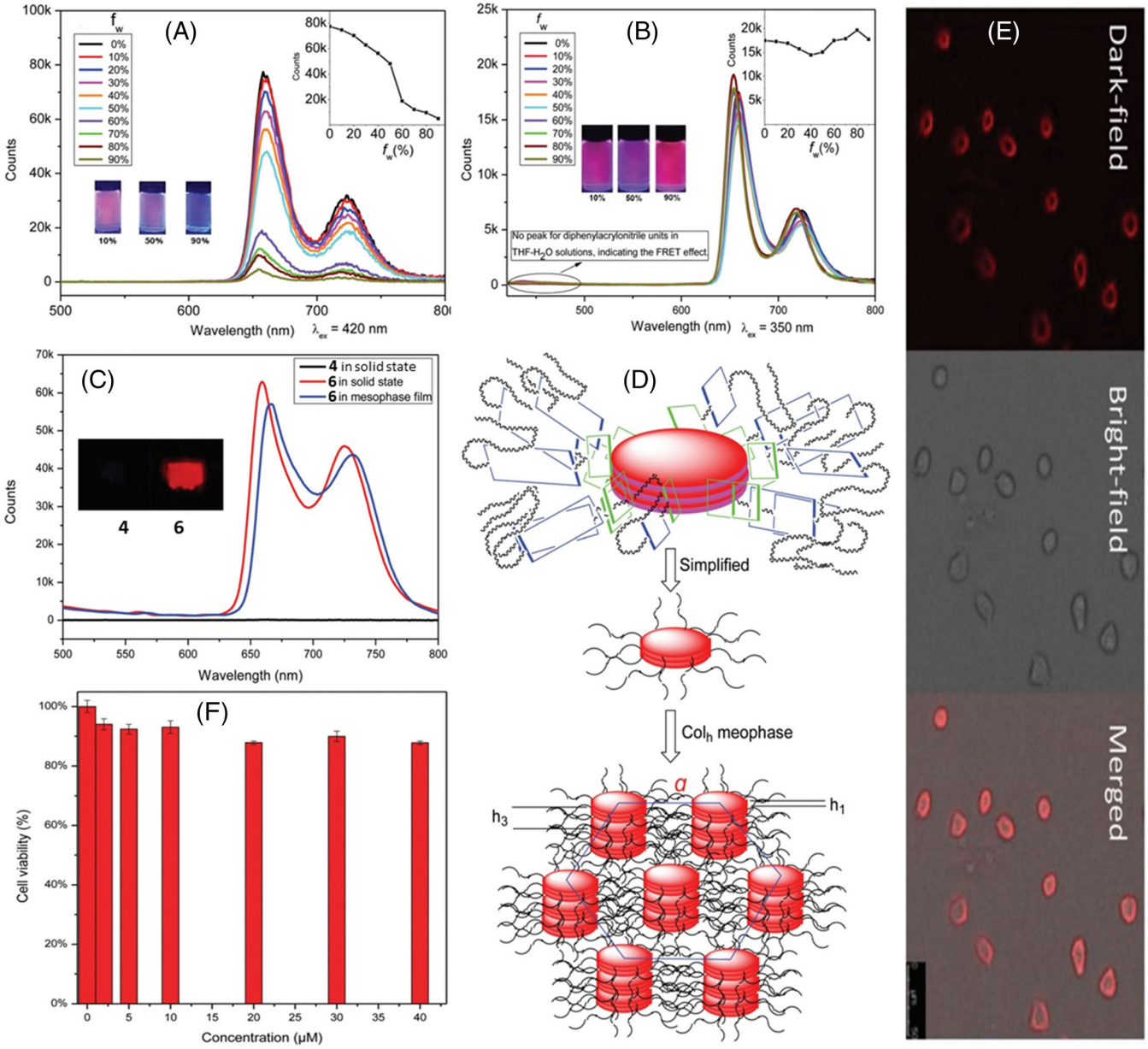

FIGURE 6 (A) Emission spectra of **6** [1 μM] in THF/H_2O mixture with different f_w (λ_{ex} = 420 nm). (B) Emission spectra of **6** [1 μM] in THF/H_2O mixture with different f_w (λ_{ex} = 350 nm). (C) Emission spectra of **4** (solid state), **6** (solid state), and **6** (mesophase film) (λ_{ex} = 350 nm); inset depicts the fluorescence photos of **6** and **4**. (D) Proposed molecular stacking mode for the hexagonal columnar mesophase of **6**. (E) Dark-field, bright-field, and merged images of fluorescence imaging in vitro HeLa cells after the incubation with porphyrin **6** for 2 h. (F) Relative cell viabilities of HeLa cells incubated with different concentrations of **6** for 24 h. Parts (A–F): Reproduced with permission.[58] Copyright 2019, Royal Society of Chemistry

self-assemblies between 70°C and 120°C (Figure 6D). Moreover, due to cooperative FRET and AIE, porphyrin **6** exhibited strong photoluminescence in the solid state and mesophase film when excited at 350 nm (Figure 6C). Under the same conditions, contrarily, the controlled porphyrin **4** showed no emission in the solid state. Furthermore, the emission peaks of porphyrin **6** were slightly red-shifted in mesophase compared to those in the solid state due to the *J*-aggregation of **6** in the mesophase state. Since porphyrin **6** exhibited a strong emission in the solid state, it was used to examine the fluorescence imaging in vitro HeLa cells. It was observed that a strong red fluorescence imaging was observed for HeLa cells containing porphyrin **6** (Figure 6E). On the other hand, the metabolic activity of HeLa cell containing porphyrin **6** was examined with an MTT assay. The results indicate that cell viabilities were over 90% at 0–40 mM in 24 h indicative of low biotoxicity for porphyrin **6** (Figure 6F). This could be attributed to the excellent biocompatibility of polyglycol chains on the periphery of AIEgen DAN.

2.2 | Photodynamic therapy

In PDT, under light irradiation, a photosensitizer is photoexcited and the photoexcited photosensitizer produces ROSs of mostly singlet oxygen ($^1O_2$) which would destroy abnormal cells.[59] This technic has been widely applied in anticancer and antibacterial fields over the past few decades. More recently, photosensitizers with bright fluorescence attracted much interest in fluorescence image-guided PDT owing to the advantages of cost-effectiveness, outstanding sensitivity, tremendous temporal resolution, and noninvasive

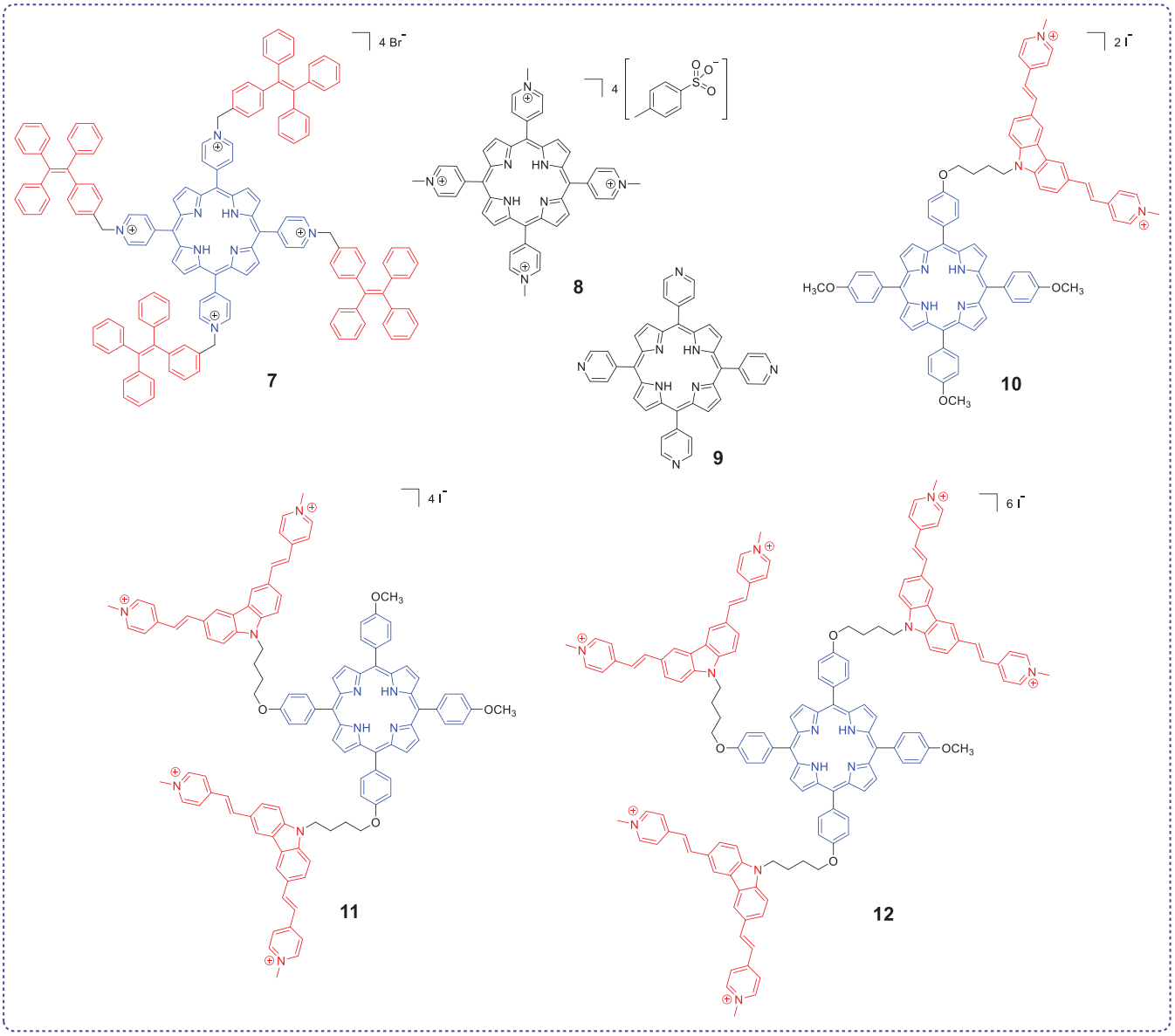

FIGURE 7 Structures of AIEgen-decorated porphyrins and related controlled porphyrins used in PDT

and real-time imaging ability.[60,61] However, hydrophobic porphyrin-based photosensitizers often suffered from ACQ because of strong π–π stacking and the formation of aggregates in aqueous solution and in cells and tissues as well. As a result, they showed a reduced fluorescence emission and thus low ROS generation. Moreover, such aggregates can also further reduce the interaction between photosensitizers and intracellular proteins which subsequently results in low PDT efficiency. To overcome the above difficulties, a few researchers designed and synthesized H_2O soluble AIEgen-decorated porphyrins and tested the PDT efficiency. The reported AIEgen-decorated porphyrins for PDT are shown in Figure 7.

The first H_2O-soluble TPE-integrated porphyrin **7** was synthesized in a one-step reaction by Wang et al.[62] The presence of four bulky TPE units efficiently hampered the π–π stacking of porphyrin molecules and impeded the ACQ in an aqueous solution. Also, the four pyridinium salts of **7** provided good solubility in an aqueous solution. The capability of $^1O_2$ generation of **7** was estimated using the decomposition rate of *N*,*N*′-di-(2,3-dihydroxypropyl)-9,10-anthracenedipropanamide (DHPA) in phosphate-buffered saline (PBS) (pH = 7.4). It was noticed that **7** displayed a high Φ_Δ of 0.85, which is much higher than those of reference compounds **8** (0.74) and **9** (0.03). Additionally, **7** showed good photostability, which was verified by a 10% decrement in the emission intensity of **7** after 80 min light irradiation (Figure 8A). Furthermore, **7** showed a high binding ability to proteins making it a highly efficient protein photocleaving agent. As a consequence of the high Φ_Δ and high binding ability, **7** was employed as a photosensitizer in PDT under light irradiation. The results confirmed that **7** effectively cleaved the bovine serum albumin and lysozyme, demonstrating the promising photosensitizing action of **7**. On the other hand, the applicability of the **7** molecule in photodynamic anticancer and photodynamic antimicrobial activity is also feasible in the future due to very good solubility and high Φ_Δ in aqueous solution.

Three binary molecular conjugates, **10–12** containing BMVC energy donor and mono-, bis-, and tris-hydroxyl porphyrin energy acceptor were synthesized by Chang et al., who investigated on the AIE and PDT properties of

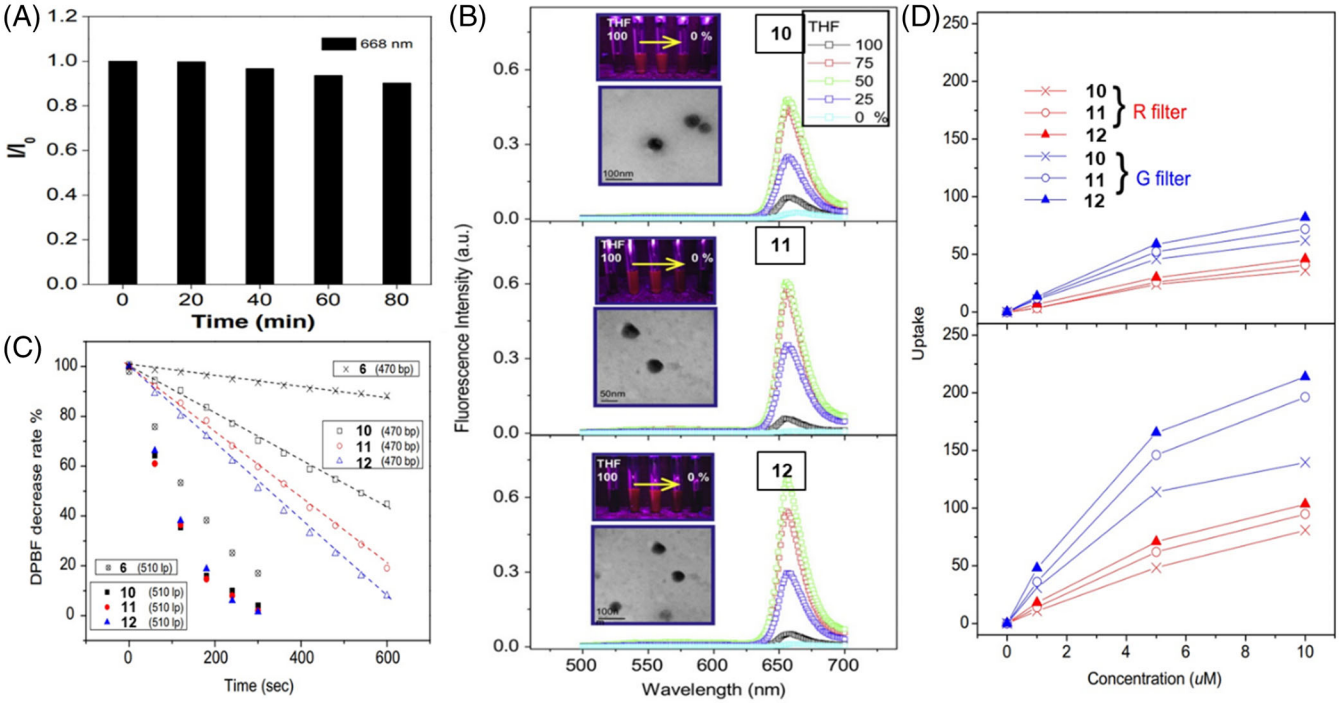

FIGURE 8 (A) Photostability of **7**. (B) Emission spectra of **10–12** (10 μM and λ_{ex} = 470 nm) recorded in THF/H_2O with different f_w; inset photos depict the visible emission photographs under UV light (365 nm) and corresponding TEM images. (C) Relative rates of DPBF oxidation by $^1O_2$ that was generated from **10–12** and **6** after irradiation with a 20 W Xenon lamp. (D) Intracellular **10–12** accumulation in normal (MRC-5) (top) and cancer (HeLa) (bottom) cells. Part (A): Reproduced with permission.[62] Copyright 2019, Elsevier SD. Parts (B–D): Reproduced with permission.[63] Copyright 2012, Elsevier SD

fluorescent organic nanoparticles (FONs) of **10–12**.[63] In the absorption spectra (in dimethyl sulfoxide), ε of absorption peaks belonging to the porphyrin unit showed a similar trend for all these molecules, while notable changes were found in the ε value of the absorption peaks (ca. 470 nm) which correspond to the BMVC entity due to different compositions of BMVC units in the molecules. These molecules can be considered as amphiphilic binary conjugates, since the anisole group of porphyrins signifies the hydrophobic portion, whereas the BMVC represents the hydrophilic portion. Hence, the Lop P of these conjugates are in the order: **10** (2.02) > **11** (–0.31) > **12** (–1.18). When these molecules were excited at different excitation wavelengths (360–630 nm), the emission peaks at 600–750 nm belonging to the porphyrin unit were observed with no emission peak of BMVC (500–600 nm), implying an efficient FRET occurred from BMVC to porphyrin unit. The AIE nature of **10–12** was studied in THF/H_2O mixture (Figure 8B). The emission intensity of these molecules reached the maximum values at f_w = 75% and/or = 50% in THF/H_2O mixture. It specifies that these molecules contain different degrees of AIE in the THF/H_2O mixture. Moreover, the transmission electron microscopy (TEM) images of **10–12** in the THF/H_2O mixture displayed fine sphere-shaped NPs and their sizes were concentration-dependent (Figure 8B). On the other hand, no fluorescence enhancement was observed for BMVC and porphyrin precursor **4**, indicating the absence of AIE in the THF/H_2O mixture. Hence, it is reasonable to say that the FONs only come from the aggregates of **10**, **11**, and **12**. Under 510 and 470 nm excitations, the order of $^1O_2$ generation of these molecules is **12** > **11** > **10** (Figure 8C). However, the $^1O_2$ generation is more significant under 470 nm excitation. It indicates that the FRET from BMVC to porphyrin core plays a great role in $^1O_2$ generation under FON conditions. Interestingly, these conjugates were more accumulated than **4** in cells and also their accumulation in cancer cells is more prominent than in normal cells. The order of intracellular accumulation of conjugates is **12** > **11** > **10**, indicating that the accumulation was dependent on the number of BMVC moieties (Figure 8D). It was found that **11** and **12** exhibited a higher intracellular mitochondria accumulation than **10**. Contrarily, **10** showed a higher intracellular lysosome accumulation than **11** and then **12**. It signifies that these conjugates can efficiently localize in mitochondria and lysosomes for improving PDT efficiency. Furthermore, the FONs of these conjugates have much more phototoxicities to cancer cells than to normal cells with no significant dark toxicity.

2.3 | Photocatalytic hydrogen evolution

PHE has been demonstrated as a potential clean energy technology to produce green energy via artificial photosynthesis. For this purpose, porphyrins received much attention due to their high UV-visible light-harvesting ability, suitable highest occupied molecular orbital (HOMO) and lowest unoccupied molecular orbital (LUMO) energy levels for efficient hole-electron pair separation, and multiple redox states.[12] However, the PHE of these porphyrins was mostly improved by enhancing the light-harvesting ability and photoinduced charge separation.[64,65] But, improving the PHE of porphyrins through AIE was reported very uncommon. The porphyrin reported for enhanced PHE through AIE is shown in Figure 9.

Zheng et al. have recently synthesized an Ir-motif conjugated porphyrin **13** and studied its AIE property.[48] Porphyrin **13** covered the absorption from 220 to 700 nm, indicating that the conjugation of Ir-motif to the porphyrin

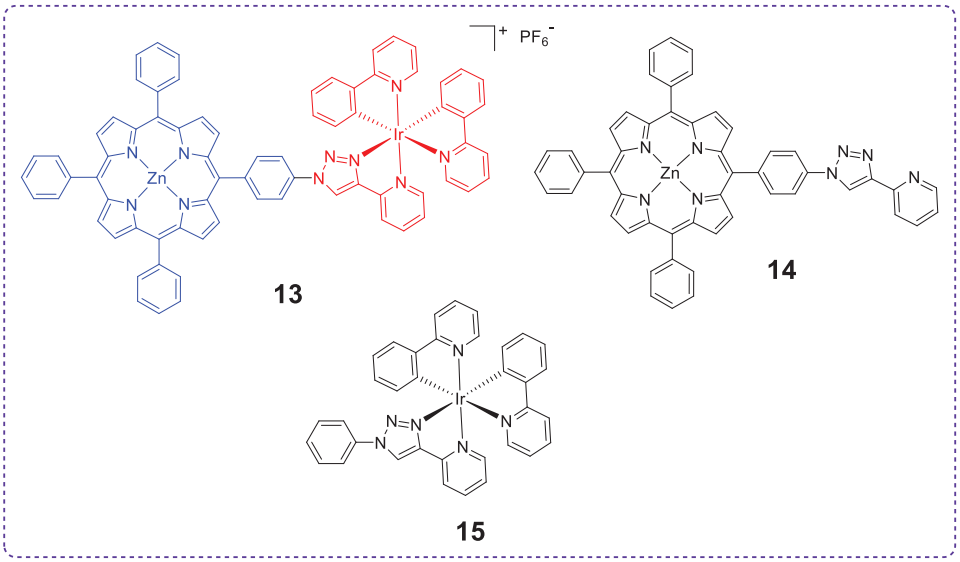

FIGURE 9 Structure of AIEgen-decorated porphyrin and related controlled molecules used in PHE

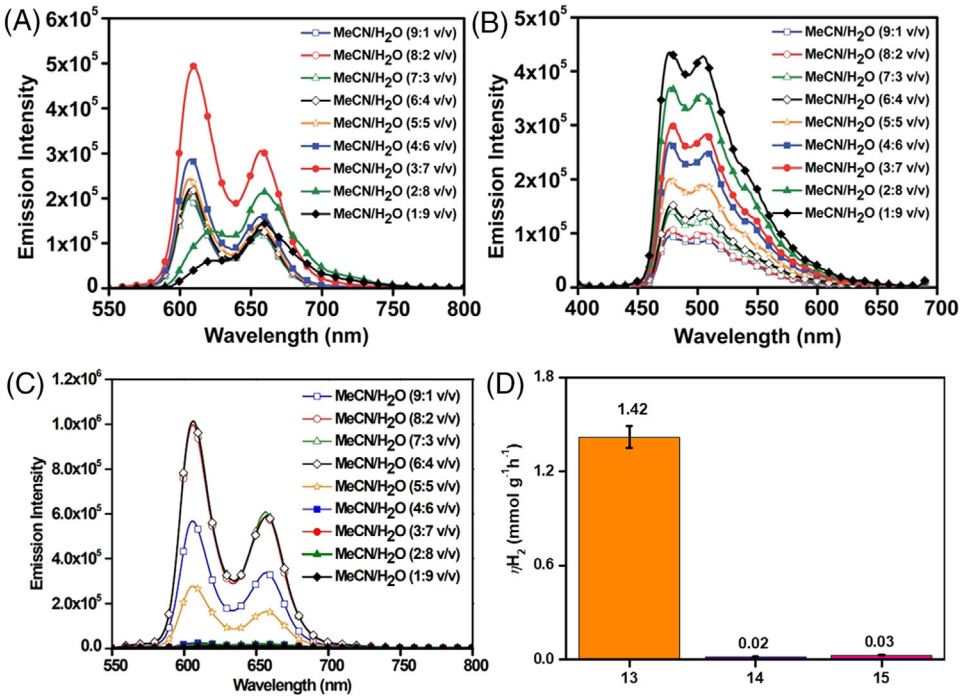

FIGURE 10 Emission spectra of (A) **13** (10 μM, λ_{ex} = 420 nm), (B) **15** (10 μM, λ_{ex} = 350 nm), and (C) **14** (10 μM, λ_{ex} = 420 nm) in ACN/H_2O with different f_w. (D) ηH_2 of **13**, **14**, and **15** under irradiation for 5 h: **13–15** (10 μM) + TEOA (0.8 M) + ACN/H_2O (1:9, v/v). Parts (A–C): Reproduced with permission.[48] Copyright 2022, Royal Society of Chemistry

ring is a facile strategy to enhance the light-harvesting property. It was found that the conjugation of Ir-motif to the porphyrin ring hampered the ACQ and provided the AIE property. Moreover, the Ir-motif not only offered the AIE property for **13** in acetonitrile (ACN)/H_2O mixture (Figure 10A) but also FRET from the Ir-motif to the porphyrin ring and consequently improved the photoexcited state lifetimes of porphyrin **13**. Notably, porphyrin **14** which lacks the Ir-motif exhibited ACQ (Figure 10C), and Ir-complex **15** without porphyrin macrocycle was an excellent AIE molecule in ACN/H_2O mixture (Figure 10B). This porphyrin produced a hydrogen evolution rate (ηH_2) of 1.42 mmol g^{-1} h^{-1} when applying it as a photosensitizer in the PHE system without a cocatalyst. The ηH_2 of **13** was much higher than that of the controlled porphyrin **14** (0.02 mmol g^{-1} h^{-1}) and Ir-complex **15** (0.03 mmol g^{-1} h^{-1}) (Figure 10D). The higher ηH_2 of **13** than **14** and **15** could be attributable to the cooperative effect of AIE, ACQ inhibition, and FRET, leading to improved UV-visible light-harvesting, populated photoexcited states with a longer electron lifetime, and thus enhanced electron transfer from the porphyrin photoexcited states to proton.

2.4 | Miscellaneous

In addition, some AIEgen-decorated porphyrins were also used in ECL, circularly polarized luminescence (CPL),

solid state luminescence, and self-assembled superstructure studies. Those reported porphyrins for the above applications are shown in Figures 12 and 14.

Rananaware et al. synthesized two TPE-based star-shaped porphyrins **16** and **17** and investigated their photophysical and redox properties, and supramolecular self-assemblies through solvophobic effect.[66] In the chloroform ($CHCl_3$) solution, both porphyrins have shown a red-shifted absorption profile than their analogs **18** and **19** without TPE moieties which could be attributed to an elongated π-conjugation between TPE chromophores and porphyrin skeleton. Similarly, the Φ_{PL} of **16** and **17** were calculated to be 15% and 12%, respectively, which were higher than those of **18** and **19**. This could be ascribed to the more rigid structures of **16** and **17** with the TPE conjugation that reduced the vibrational decay of excited states effectively. Moreover, the absorption and emission spectra of **16** were recorded in nonpolar and polar organic solvent mixtures, such as $CHCl_3$/MeOH (1:1, v/v) and $CHCl_3$/cyclohexane (1:1, v/v) to understand the nature of aggregation. It was noticed that the absorption (Soret-band) and emission peaks were red-shifted in $CHCl_3$/MeOH (1:1, v/v) and blue-shifted in $CHCl_3$/cyclohexane (1:1, v/v), indicating a *J*- and *H*-type of aggregation, respectively, via π–π stacking interactions between the aromatic cores of **16**. This result also further corroborates that solvophobicity plays a major role in the formation of different types of aggregates. However, porphyrin **17** did not show the above results due to the presence of Zn metal. The TEM image illustrates that compound **16** was aggregated into well-defined ring-like nanostructures in $CHCl_3$/MeOH (1:1, v/v), and the sizes of the ring-like nanostructures were found to be 0.25, 0.50, and 0.75 μm, attributing to the increment in thickness of the porphyrin nanostructures (Figure 11A). This result also matches with the dynamic light scattering (DLS) output, where different sizes of particles were observed (Figure 11C). Contrarily, well-defined spherical aggregates with a size range from 150 to 300 nm were found in $CHCl_3$/cyclohexane (1:1, v/v) (Figure 11B). More interestingly, different morphologies, such as honeycombs, sheets, and amorphous particles, were observed for **16** when varying either the concentration of **16** or the amount of MeOH/cyclohexane. These results indicate that a subtle balance existed between the solvophobicity and concentration of porphyrin **16** to form a well-defined nanostructure. Especially, the self-assembled ring-shaped morphology of **16** can act as a good material for the construction of light-harvesting nanodevices.

Two new porphyrins **20** and **21** containing bulky *tert*-butylthio-substituents were designed and synthesized by Zhang et al. and they studied on their AIE properties.[34] For both porphyrins, the Soret-band was red-shifted with a low ε when increasing f_w from 0% to 90% in THF/H_2O mixed solution. It indicates that both porphyrins were arranged in an edge-to-edge direction which resulted in the *J*-aggregates. The emission spectra revealed that the intensity of emission peaks increased gradually when increasing the f_w from 0% to 55% and then declined from 60% to 90% for **20** (Figure 11H). On the other hand, **21** exhibited first an increased emission intensity from 0% to 70% of f_w and then a decreased emission intensity from 80% to 90% with increasing f_w (Figure 11I). These outcomes clearly demonstrate that the increased intermolecular steric effects of bulky substituents result in the reduced π–π stacking interactions between the porphyrin units and thus the formation of well-ordered *J*-aggregates with an enhanced emission in THF/H_2O mixed solution. The SEM results reveal that two-dimensional nanosheets at f_w = 55% (Figure 11D) and irregularly shaped NPs of **20** were observed at f_w = 90% (Figure 11E), whereas regular nanorods and irregular NPs of **21** were formed at f_w = 70% and 90%, respectively (Figure 11F,G). Finally, the photophysical and morphological studies demonstrate that the introduction of the bulky *tert*-butylthio-substituents into the porphyrin core is a simple molecular design strategy to enhance the emission intensity in the aggregated state of porphyrins.

Zhang et al. synthesized a liposoluble porphyrin **22** containing a TPE unit and studied the AIE property and ECL.[52] The emission intensity of this porphyrin was gradually increased with rising f_w from 0% to 90% in dimethylformamide (DMF)/H_2O mixture, indicating an AIE property of **22** (Figure 13B). It means the TPE chromophore in **22** effectively suppressed the strong π–π-stacking of porphyrin molecules in the aggregated state and thus reduced the nonradiative deactivation of the photoexcited states of **22**. Noteworthily, the intensity of emission peaks of **22** is higher than that of **23** without the TPE unit (Figure 13A). This could be ascribed to the FRET from the TPE energy donor to the porphyrin ring energy acceptor in **22**. When compared to the absorption spectra of **22** in the DMF solution, the absorption spectra of **22** in DMF/H_2O mixture (f_w = 90%) were red-shifted (Figure 13A). It indicates that **22** tended to assemble into *J*-aggregates and thus head-to-head aggregate form was assigned to **22**, in which TPE moiety was assigned as the "head". whereas porphyrin core as the "tail". The differential pulse voltammetric technic and DFT calculations demonstrate that the HOMO and LUMO energy gap of **22** is smaller than that of **23**. This result indicates that conjugation of TPE moiety to the porphyrin core could improve the electron delocalization and thus decreased the HOMO-LUMO energy gap for **22**. Under the conditions of 0.1 M $K_2S_2O_8$ coreactant in 0.1 M PBS (pH = 7.5) solution with 0.1 M KCl supporting electrolyte, ECL studies point out that the intensity of ECL peak of **22** is six-fold higher than that of **23**, signifying **22** is a potential candidate for generating ECL in aqueous phase (Figure 13D). Moreover, **22** displayed a very weak ECL peak at $f_w \leq 20\%$, whereas the intensity of the ECL peak increases with increasing f_w from 20% to 90%, indicating the aggregation-induced ECL of **22** in aqueous solution (Figure 13D). The ECL of **22** seems to be constant even after 20 cycles (Figure 13F), denoting good aggregation-induced electrochemiluminescence (AIECL) reproducibility and stability.

Wang et al. designed and synthesized a new porphyrin **24** with chiroptical properties in the aggregated state.[67] In **24**, the porphyrin core acts as an energy acceptor and DAN containing peripheral chiral alkyl chain acts as an energy donor. This porphyrin possesses a strong FRET feature from DAN units to the porphyrin core due to the overlapped emission peak of DAN at 400–520 nm and the Soret-band absorption peak of porphyrin at 400–450 nm. Similarly, the strong emission peak of DAN disappeared and only porphyrin emission peaks at 630–750 nm were observed when **24** was excited at 340 nm which corresponds to the DAN absorption (Figure 13H). Similar to porphyrin **4**, when excited at 420 nm

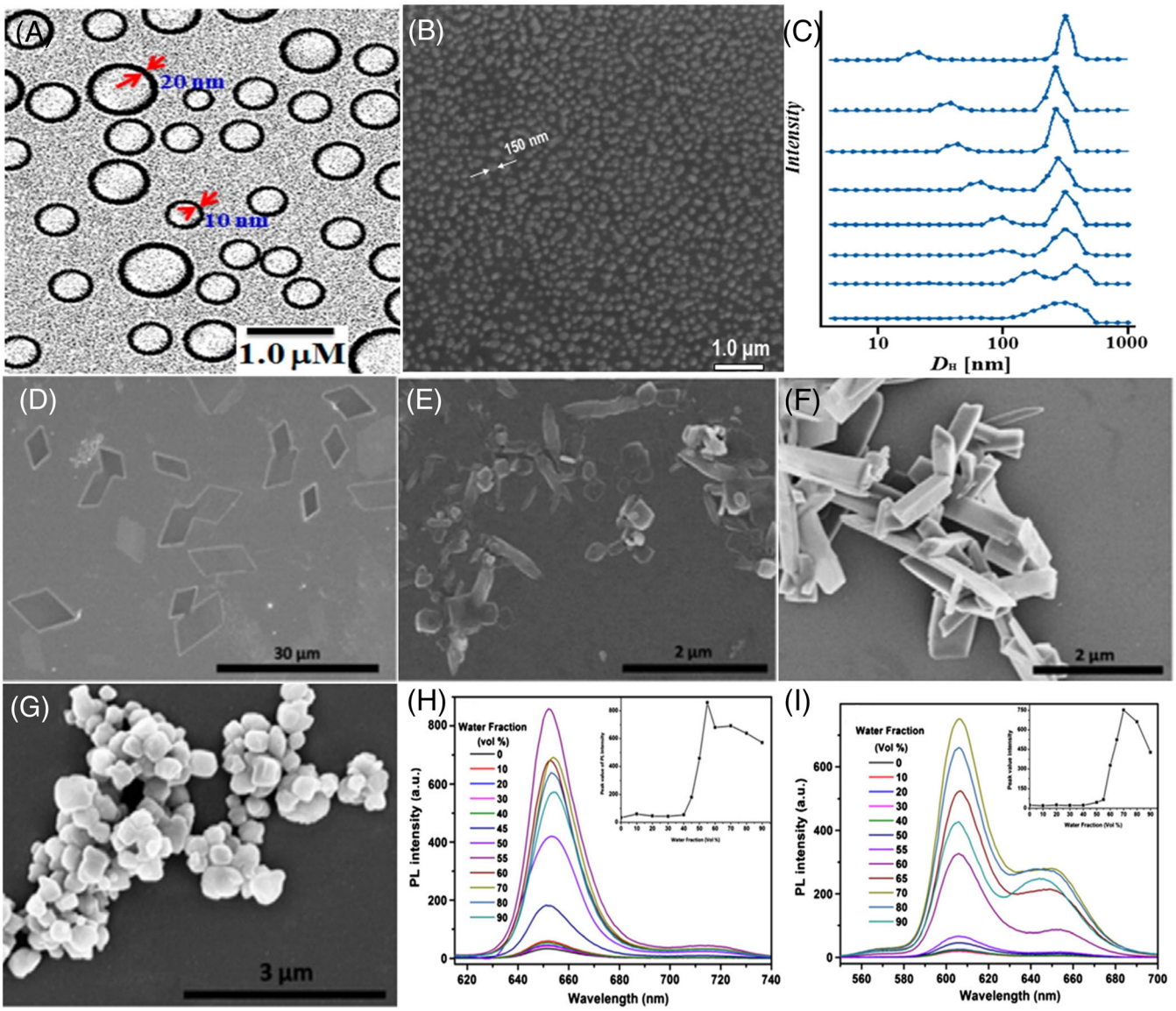

FIGURE 11 (A) TEM images on a carbon-coated copper grid of **16** (10^{-4} M) in $CHCl_3$/MeOH (1:1, v/v). (B) SEM of **16** (10^{-4} M) in $CHCl_3$/cyclohexane (1:1, v/v). (C) Time-dependent DLS measurements of **16** (10^{-4} M) solutions in $CHCl_3$/MeOH (1:1, v/v). SEM images of **20** in THF/H_2O mixture (D) at f_w = 55% and (E) f_w = 90%. SEM images of **21** in THF/H_2O mixture (F) at f_w = 70% and (G) at f_w = 90%. Emission spectra of (H) **20** and (I) **21** in THF/H_2O mixture with different f_w; inset depicts changes of emission intensity with different f_w. Parts (A–C): Reproduced with permission.[66] Copyright 2015, American Chemical Society. Parts (D–I): Reproduced with permission.[34] Copyright 2014, Elsevier SD

belonging to the absorption of porphyrin core, **24** showed a very strong ACQ with an increase of f_w in THF/H_2O mixture (Figure 13G). Contrarily, an appreciable AIE property was observed for **24** in f_w > 40% in THF/H_2O mixture under the excitation of 340 nm, that is, related to the DAN absorption. This could be explained in such a way that under a balanced f_w in THF/H_2O mixture, a strong FRET from the DAN units to the porphyrin core induces the AIE in **24** when excited at 340 nm. Furthermore, differential scanning calorimetry experiments reveal that **24** displayed phase transition temperatures at 62.5°C and 113.2°C under heating and at 58.3°C and 108.5°C upon cooling, signifying the good liquid crystalline property of crystalline-mesophase-isotropic transition. X-ray diffraction data further support that **24** possesses an ordered hexagonal columnar mesophase. Later, **24** exhibited apparent circular dichroism (CD) typical signals at 320–360 nm and 400–430 nm under AIE conditions, solid state, and mesophase, and these signals are consistent with the characteristic absorption bands of **24**. On the other hand, **24** showed CPL signals at about 650–850 nm under AIE conditions, solid state, and mesophase, and these signals match with the characteristic emission peaks of **24**. All these results speculate that an effective chirality transfer from the chiral alkyl chains to both achiral DAN units and porphyrin moiety in aggregated states of **24**. The order of intensity of CD signals of **24** in different media is THF/H_2O mixture < solid film < mesophase, representing the highest order degree in the mesophase. Similarly, the CPL asymmetry factor (g_{lum}) values of **24** also followed the order of THF/H_2O mixture ($|-3.5 \times 10^{-3}|$) < solid film ($|-4.6 \times 10^{-3}|$) < mesophase ($|-6.6 \times 10^{-3}|$), reflecting the order of the intensity of CD signals. Overall, a highly ordered helical π–π columnar stacking structure was observed for **24** in a mesophase aggregated state and consequently, larger values of g_{lum} for CPL behavior (Figure 13I). Finally, this work demonstrates how to convert achiral porphyrins possessing the ACQ effect to bright luminescent molecules with good CPL behavior in the aggregated state.

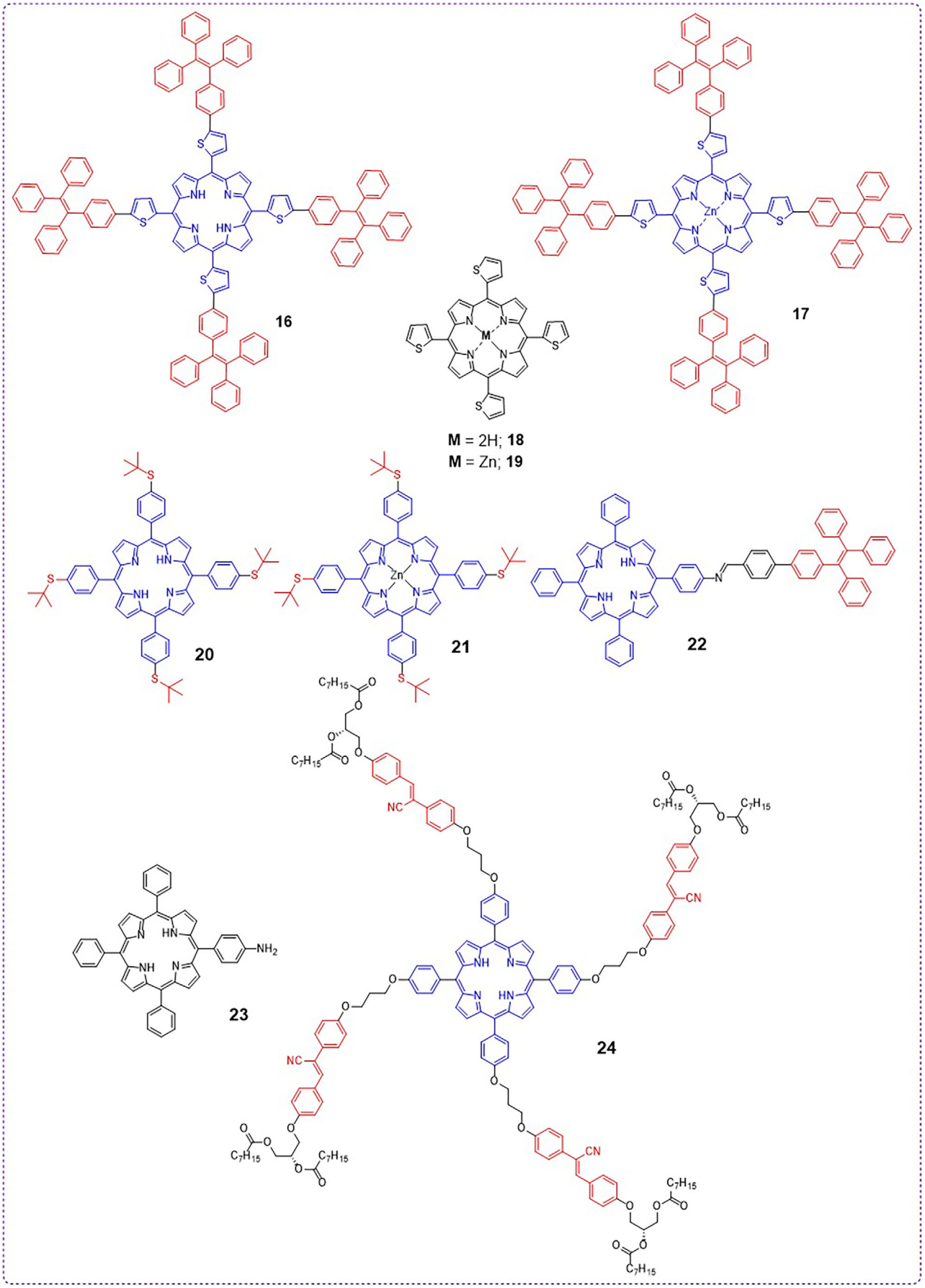

FIGURE 12 Structures of AIEgen-decorated porphyrins and related controlled porphyrins used in the self-assembled study, electrochemiluminescence, and chiroptical properties

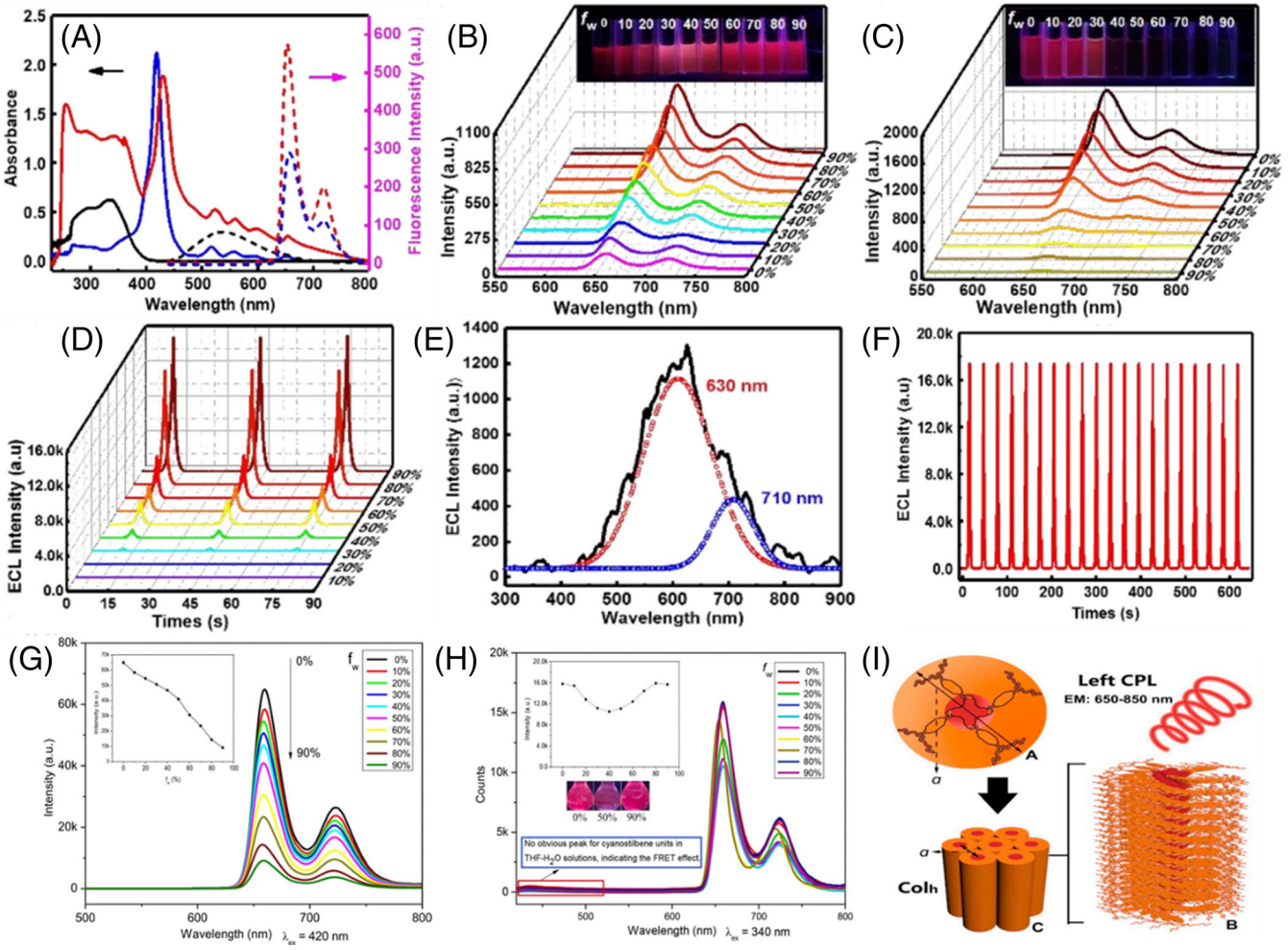

FIGURE 13 (A) Absorption (solid) and emission (dash) spectra of 5 μM DMF solution of **22** (red) and **23** (blue). Emission spectra of (B) **22** and (C) **23** in DMF/H_2O mixture with different f_w from 0% to 90%; inset shows photographs under the illumination of UV light (365 nm). (D) The ECL-time curves of 0.015 mM **22** with different f_w. (E) ECL spectrum and (F) stability test under optimal conditions. (G) Emission spectra of **24** (1 μM) in THF/H_2O mixture with different f_w (λ_{ex} = 420 nm); inset depicts the line plot of fluorescence intensity (maximum value between 650 and 670 nm) change from 0% to 90% of H_2O. (H) Emission spectra of **24** (1 μM) in THF/H_2O mixture with different f_w (λ_{ex} = 340 nm); inset depicts line plot of fluorescence intensity (maximum value between 650 and 670 nm) change from 0% to 90% of H_2O and the fluorescence photos (under UV365 light). (I) The proposed spiral molecular stacking in hexagonal columnar mesophase for **24**. Parts (A–F): Reproduced with permission.[52] Copyright 2020, Wiley-VCH GmbH. Parts (G–I): Reproduced with permission.[67] Copyright 2021, Elsevier SD

The first example of free-base and Zn(II)-tetraazaporphyrins (TAPs) **25**–**28** with TPE/DPP was developed by Tasso et al. to suppress the ACQ of TAPs in their aggregated states.[68] These TAPs exhibit strong absorption profiles from 300 to 700 nm, indicating their UV/Vis/NIR absorption. Especially, the Q-bands of Zn(II)-TAPs **26** and **28** were red-shifted by 40 nm in comparison with the analogs Mg(II) and Zn(II)-TAPs with octaphenyl-substituted TAPs, indicating their potential applications in solar cells and biomedical fields. Time-dependent (TD)-DFT calculations demonstrate that the destabilization of HOMOs and LUMOs of **26** and **28** led to a narrower HOMO and LUMO gap than the parent unsubstituted TAPs. Moreover, the broad and low intensified overlapping bands in the region of 450–600 nm of the absorption spectra of **25**–**28** are attributable to the intramolecular charge-transfer (ICT) transitions from the TPE/DPP units to the TAP ring. Also, the localization of HOMOs on TPE/DPP units and the contribution of TAP core to LUMOs clearly indicate the ICT nature of **25**–**28**. In the photoluminescence spectra, these TAPs showed strong emission peaks ranging from 670 to 770 nm, indicating their NIR-emitting behavior. However, they exhibited small Stokes shift values of ca. 15 nm. This could be ascribed to the synergetic effect of the rigid TAP core containing steric crowding TPE/DPP units, resulting in restricted molecular rearrangements in the photoexcited state. Notably, through these TAPs excited at 320 nm which corresponds to the TPE/DPP units, they only displayed fluorescence of the TAP core, indicating the good electronic communication between TPE/DPP units and the TAP core. The Φ_{PL} of these TAPs decreased when f_w increased in THF/H_2O mixture, illustrating the ACQ nature of **25**–**28**. Moreover, powders of **25**–**28** were nonemissive, indicating that the substitution of AIEgens into the TAP core is not helpful to restrict the fluorescence quenching in the solid state and consequently, short-lived charge-separated species of TAP molecules. Metal-free TAPs **25** and **27** showed much lower Φ_Δ values than their corresponding Zn(II)-TAPs **26** and **28**. Among the TAPs, **28** has a Φ_Δ value of 0.55, which replicates the value of the ZnPc standard. It indicates that **28** can be utilized as a potential photosensitizer in the PDT application.

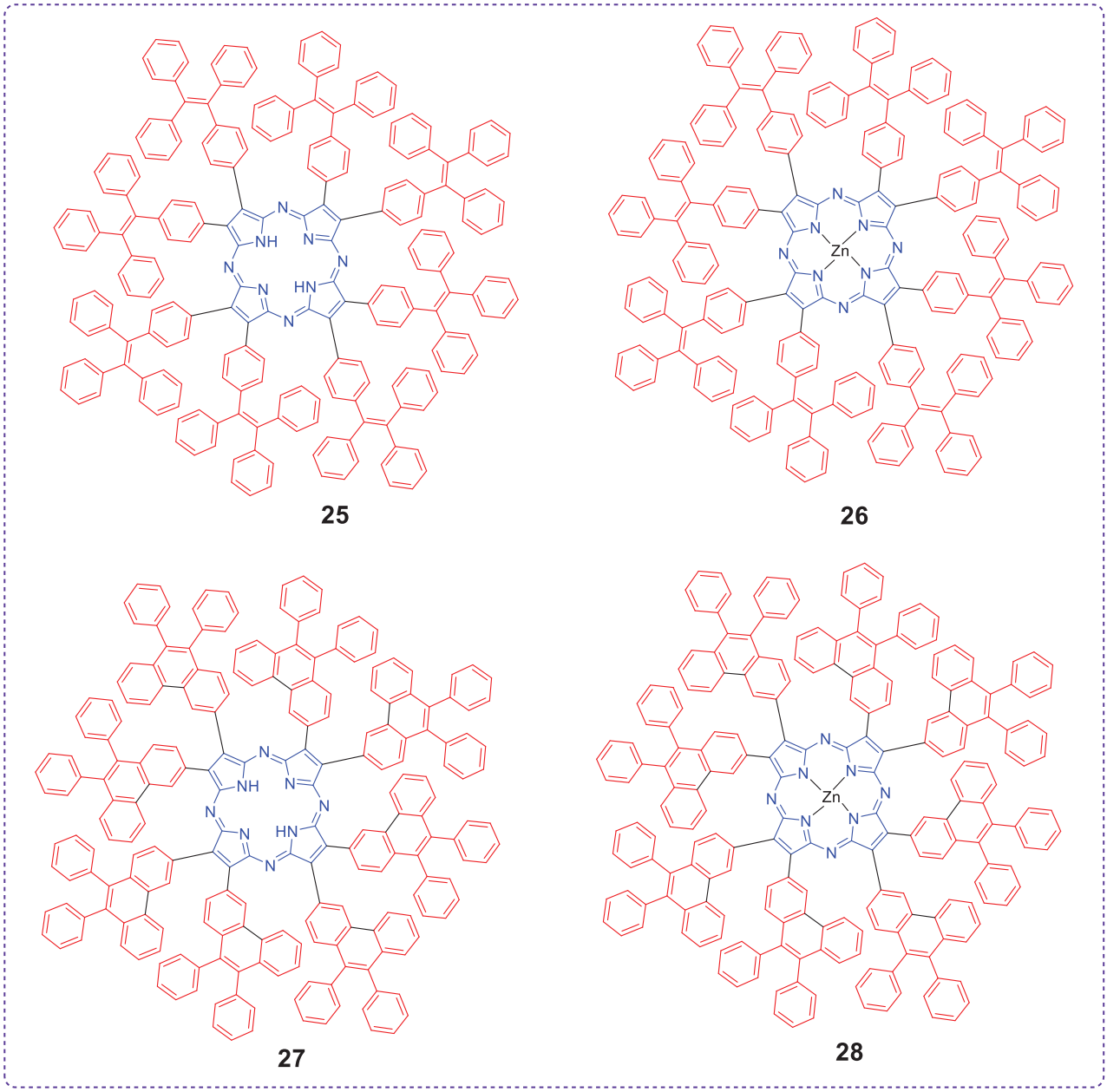

FIGURE 14 Structures of AIEgen-decorated tetraazaporphyrins (TAPs)

3 | CONCLUSIONS AND PERSPECTIVES

In conclusion, we have summarized the rational design of porphyrins containing AIEgens for NIR fluorescence bioimaging, PDT, PHE, ECL and chiroptical applications, and self-assembled studies reported to date. It was found that the introduction of AIEgens, such as TPE, DAN, and Ir-motif into the porphyrin core, induced a strong FRET from the AIEgen energy donor to the porphyrin energy acceptor due to the overlapped Soret-band absorption peaks of porphyrin core and emission peaks of AIEgens. Moreover, the bulkiness of such AIEgens motifs also converted the porphyrins from ACQ to AIE in their solid state due to the reduced strong intermolecular π–π stacking of porphyrins. Subsequently, such porphyrins with AIE were employed as potential candidates in the above-mentioned applications. Notably, most of the porphyrins showed AIE property when they were excited at AIEgens absorption, whereas, under the excitation of the porphyrin ring Soret-band absorption, ACQ was observed. This could be attributed to the fact that the FRET between the porphyrin ring and AIEgen moieties triggered the AIE. Besides, porphyrins containing TPE and DAN AIEgens showed admirable AIE in THF/H_2O mixture and consequently enhanced fluorescence bioimaging properties than controlled porphyrins without AIEgens. Similarly, H_2O-soluble porphyrins with TPE and BMVC AIEgens showed decent PDT results compared to those of porphyrins without AIEgens due to AIE and improved interaction between AIEgen-decorated porphyrins and intracellular proteins. Notably, though Ir-motif conjugated porphyrin showed some degree of AIE in ACN/H_2O, it did not show up as complete AIE. Additionally, this porphyrin is not much photostable in PHE application, indicating that the molecular design of Ir-motif conjugated porphyrin needs to be modified. In addition, porphyrins containing bulky tert-butylthio-substituents showed different degrees of AIE properties. Particularly, free-base porphyrin with bulky tert-butylthio-substituents formed two-dimensional nanosheets at f_w = 55%, while regular nanorods were noticed for Zn(II)-porphyrin with bulky tert-butylthio-substituents at f_w = 70%. These studies

demonstrate that introducing the bulky tert-butylthio-substituents onto the porphyrin core and inserting Zn metal inside the porphyrin ring were simple ways to enhance the emission intensity of porphyrins featuring defined morphology in the solid state. Furthermore, though TPE-based star-shaped porphyrins with thiophene π-linker possess TPE moieties, they did not show AIE in the aggregated state. These TPE-based star-shaped porphyrins exhibited well-defined supramolecular self-assemblies through the solvophobic effect and their morphologies were highly dependent on the polar and nonpolar solvent mixtures. However, it should be noted that there is a possibility to bring AIE properties for these kinds of porphyrins by replacing the thiophene π-linker between the porphyrin ring and TPE moieties with a phenyl π-linker. In another example, TAPs containing TPE/DPP also faced ACQ in the solid state. These results clearly indicate that an appropriate molecular design is required to achieve AIE properties for TAPs. Liposoluble TPE containing porphyrin with AIE property exhibited facile ECL performance than that of porphyrin without TPE moieties and porphyrin possessing DAN moieties comprising peripheral chiral alkyl chain displayed CPL behavior in the aggregated state.

Nevertheless, the use of AIEgen-decorated porphyrins in carbon dioxide reduction to value-added chemicals through photocatalytic or electrocatalytic ways is not reported yet, thus employing them for enhanced carbon dioxide reduction application needs to be performed. By extending conjugation in AIEgen-decorated porphyrins, it can allow them to be used as near-infrared detector applications. Porphyrins containing TPE/DAN moieties can be applied in either homogenous or heterogeneous PHE applications instead of using more synthetically challenging and commercially not viable Ir-motif conjugated porphyrins. Fluorescence sensing of metal ions in aqueous solutions will also be done by employing H_2O-soluble AIEgen-decorated porphyrins. Excitingly, the use of AIEgen-decorated porphyrins in OLED applications is not tested yet. Therefore, such porphyrins can be used as potential red emitters with enhanced performance. Last but not least, as Pd and Pt-porphyrins exhibit long-lived triplet excited states, designing and synthesizing AIEgen-decorated Pd/Pt-porphyrins can further advance their photocatalytic and biomedicine applications where the triplet states of porphyrins play a major role.

ACKNOWLEDGMENTS

W.-Y. W. acknowledges the financial support from the Science, Technology and Innovation Committee of Shenzhen Municipality (JCYJ20180507183413211), the RGC Senior Research Fellowship Scheme (SRFS2021-5S01), the National Natural Science Foundation of China (52073242), the Hong Kong Polytechnic University, Research Institute for Smart Energy (RISE) (CDAQ), and Miss Clarea Au for the Endowed Professorship in Energy (847S). The research was supported by the General Research Fund (HKBU 12304320) from the Hong Kong Research Grants Council, and Initiation Grant for Faculty Niche Research Areas (IG-FNRA) (2020/21)-RC-FNRA-IG/20-21/SCI/06 from Research Committee of Hong Kong Baptist University.

CONFLICT OF INTEREST STATEMENT

The authors declare no conflict of interest.

ORCID

Govardhana Babu Bodedla https://orcid.org/0000-0002-8561-2713
Wai-Yeung Wong https://orcid.org/0000-0002-9949-7525

REFERENCES

1. G. B. Bodedla, H. Wang, S. Chang, S. Chen, T. Chen, J. Zhao, W.-K. Wong, X. Zhu, *ChemistrySelect* **2018**, *3*, 2558–2564.
2. V. Piradi, F. Yan, X. Zhu, W.-Y. Wong, *Mater. Chem. Front.* **2021**, *5*, 7119–7133.
3. A. Mahmood, J.-Y. Hu, B. Xiao, A. Tang, X. Wang, E. Zhou, *J. Mater. Chem. A* **2018**, *6*, 16769–16797.
4. G. B. Bodedla, X. Zhu, Z. Zhou, W.-Y. Wong, *Top. Curr. Chem.* **2022**, *380*, 49.
5. W. Yu, W. Zhen, Q. Zhang, Y. Li, H. Luo, J. He, Y. Liu, *ChemMedChem* **2020**, *15*, 1766–1775.
6. M. H. Akhter, J. Ahmad, M. N. Javed, R. Haque, H. Khalilullah, M. Gupta, J. Ali, in *Cancer Nanotheranostics*: *Volume 1* (Eds. M. Saravanan, H. Barabadi), Springer International Publishing, Cham, **2021**, pp. 275–295.
7. P. S. Chelushkin, J. R. Shakirova, I. S. Kritchenkov, V. A. Baigildin, S. P. Tunik, *Dalton Trans*. **2022**, *51*, 1257–1280.
8. M. Imran, M. Ramzan, A. K. Qureshi, M. A. Khan, M. Tariq, *Biosensors* **2018**, *8*, 95.
9. G. B. Bodedla, Y. Dong, G. Tang, J. Zhao, F. Zhang, X. Zhu, W.-Y. Wong, *J. Mater. Chem. A* **2022**, *10*, 13402–13409.
10. G. B. Bodedla, J. Huang, W.-Y. Wong, X. Zhu, *ACS Appl. Nano Mater*. **2020**, *3*, 7040–7046.
11. G. B. Bodedla, L. Li, Y. Che, Y. Jiang, J. Huang, J. Zhao, X. Zhu, *Chem. Commun.* **2018**, *54*, 11614–11617.
12. J. S. O'Neill, L. Kearney, M. P. Brandon, M. T. Pryce, *Coord. Chem. Rev.* **2022**, *467*, 214599.
13. J. Min Park, J. H. Lee, W.-D. Jang, *Coord. Chem. Rev.* **2020**, *407*, 213157.
14. D. N. Tritton, G. B. Bodedla, G. Tang, J. Zhao, C.-S. Kwan, K. C.-F. Leung, W.-Y. Wong, X. Zhu, *J. Mater. Chem. A* **2020**, *8*, 3005–3010.
15. L. Yang, Y. Cheng, D. Fan, Z. Li, *Energy Fuels* **2022**, *36*, 11292–11307.
16. Z. Liang, H.-Y. Wang, H. Zheng, W. Zhang, R. Cao, *Chem. Soc. Rev.* **2021**, *50*, 2540–2581.
17. E. Nikoloudakis, I. López-Duarte, G. Charalambidis, K. Ladomenou, M. Ince, A. G. Coutsolelos, *Chem. Soc. Rev.* **2022**, *51*, 6965–7045.
18. Z.-L. Qi, Y.-H. Cheng, Z. Xu, M.-L. Chen, *Int. J. Mol. Sci.* **2020**, *21*, 5839.
19. D. Klyamer, R. Shutilov, T. Basova, *Sensors* **2022**, *22*, 895.
20. C. Fu, X. Sun, G. Zhang, P. Shi, P. Cui, *Inorg. Chem.* **2021**, *60*, 1116–1123.
21. G. Sallam, S. Y. Shaban, A. Nassar, M. E. El-Khouly, *Spectrochim. Acta A: Mol. Biomol. Spectrosc.* **2020**, *241*, 118609.
22. D. D. La, H. H. Ngo, D. D. Nguyen, N. T. Tran, H. T. Vo, X. H. Nguyen, S. W. Chang, W. J. Chung, M. D.-B. Nguyen, *Coord. Chem. Rev.* **2022**, *463*, 214543.
23. F. Zheng, C. S. Hsu, Y. Zhang, Y. Sun, Y. Wu, H. Lu, X. Sun, Q. Shi, *Energy Fuels* **2018**, *32*, 10382–10390.
24. M. Tahoun, C. T. Gee, V. E. McCoy, P. M. Sander, C. E. Müller, *RSC Adv*. **2021**, *11*, 7552–7563.
25. J. L. Grimland, C. Wu, R. R. Ramoutar, J. L. Brumaghim, J. McNeill, *Nanoscale* **2011**, *3*, 1451–1455.
26. S. Li, K. Chang, K. Sun, Y. Tang, N. Cui, Y. Wang, W. Qin, H. Xu, C. Wu, *ACS Appl. Mater. Interfaces* **2016**, *8*, 3624–3634.
27. A. V. Kondrashina, R. I. Dmitriev, S. M. Borisov, I. Klimant, I. O'Brien, Y. M. Nolan, A. V. Zhdanov, D. B. Papkovsky, *Adv. Funct. Mater.* **2012**, *22*, 4931–4939.
28. C. Wu, B. Bull, K. Christensen, J. McNeill, *Angew. Chem. Int. Ed.* **2009**, *48*, 2741–2745.
29. E. Aguilar-Ortíz, N. Lévaray, M. Vonlanthen, E. G. Morales-Espinoza, Y. Rojas-Aguirre, X. X. Zhu, E. Rivera, *Dyes Pigm*. **2016**, *132*, 110–120.
30. T. Yamaguchi, T. Kimura, H. Matsuda, T. Aida, *Angew. Chem. Int. Ed.* **2004**, *43*, 6350–6355.
31. C. Aggelidou, T. A. Theodossiou, K. Yannakopoulou, *Photochem. Photobiol.* **2013**, *89*, 1011–1019.
32. M. Wu, Z.-W. Yu, Y. Liu, D.-F. Feng, J.-J. Yang, X.-B. Yin, T. Zhang, D.-Y. Chen, T.-J. Liu, X.-Z. Feng, *ChemBioChem* **2013**, *14*, 979–986.

33. F. Lv, X. He, L. Lu, L. Wu, T. Liu, *J. Porphyr. Phthalocyanines* **2011**, *15*, 217–222.
34. G. Zhang, Q. Chen, Y. Zhang, L. Kong, X. Tao, H. Lu, Y. Tian, J. Yang, *Inorg. Chem. Commun.* **2014**, *46*, 85–88.
35. M.-C. Hsieh, C.-H. Chien, C.-C. Chang, T.-C. Chang, *J. Mater. Chem. B* **2013**, *1*, 2350–2357.
36. B. Huang, Y. Cheng, H. Lei, L. Hu, Z. Li, X. Huang, L. Chen, Y. Chen, *Chem. Commun.* **2021**, *57*, 4015–4018.
37. K.-H. Ong, B. Liu, *Molecules* **2017**, *22*, 897.
38. A. Pucci, in *Aggregation-Induced Emission (AIE)*, Elsevier, **2022**, pp. 427–447.
39. Q. Wei, J. Zhang, Z. Ge, *Handbook of Aggregation-Induced Emission*, **2022**, pp. 1–26.
40. F. Rizzo, F. Cucinotta, *Isr. J. Chem.* **2018**, *58*, 874–888.
41. J. Hwang, P. Nagaraju, M. J. Cho, D. H. Choi, *Aggregate* **2023**, *4*, e199.
42. D. Ma, in *Aggregation-Induced Emission*, Springer International Publishing, Cham, **2022**, pp. 171–207.
43. J. Wang, Q. Meng, Y. Yang, S. Zhong, R. Zhang, Y. Fang, Y. Gao, X. Cui, *ACS Sensors* **2022**, *7*, 2521–2536.
44. M. Asad, M. Imran Anwar, A. Abbas, A. Younas, S. Hussain, R. Gao, L.-K. Li, M. Shahid, S. Khan, *Coord. Chem. Rev.* **2022**, *463*, 214539.
45. P. Zhou, K. Han, *Aggregate* **2022**, *3*, e160.
46. D. Dai, J. Yang, Y.-W. Yang, *Chem. Eur. J.* **2022**, *28*, e202103185.
47. N. Meher, D. Barman, R. Parui, P. K. Iyer, *J. Mater. Chem. C* **2022**, *10*, 10224–10254.
48. K. Zheng, G. B. Bodedla, Y. Hou, J. Zhang, R. Liang, J. Zhao, D. Lee Phillips, X. Zhu, *J. Mater. Chem. A* **2022**, *10*, 4440–4445.
49. J. Wang, L. Zhang, Z. Li, *Adv. Healthc. Mater.* **2021**, *10*, 2101169.
50. X. Zhang, K. Wang, M. Liu, X. Zhang, L. Tao, Y. Chen, Y. Wei, *Nanoscale* **2015**, *7*, 11486–11508.
51. L. Huang, L. Dai, *J. Polym. Sci. Part A: Polym. Chem.* **2017**, *55*, 653–659.
52. Y. Zhang, Y. Zhao, Z. Han, R. Zhang, P. Du, Y. Wu, X. Lu, *Angew. Chem. Int. Ed.* **2020**, *59*, 23261–23267.
53. Z. Guo, S. Park, J. Yoon, I. Shin, *Chem. Soc. Rev.* **2014**, *43*, 16–29.
54. J. O. Escobedo, O. Rusin, S. Lim, R. M. Strongin, *Curr. Opin. Chem. Biol.* **2010**, *14*, 64–70.
55. B. Guo, X. Cai, S. Xu, S. M. A. Fateminia, J. Liu, J. Liang, G. Feng, W. Wu, B. Liu, *J. Mater. Chem. B* **2016**, *4*, 4690–4695.
56. Q. Yu, S. Chen, C. Han, H. Guo, F. Yang, *J. Lumin.* **2020**, *220*, 117017.
57. C. Han, S. Jiang, J. Qiu, H. Guo, F. Yang, *New J. Chem.* **2019**, *43*, 3317–3322.
58. H. Guo, S. Zheng, S. Chen, C. Han, F. Yang, *Soft Matter* **2019**, *15*, 8329–8337.
59. H. Yu, B. Chen, H. Huang, Z. He, J. Sun, G. Wang, X. Gu, B. Z. Tang, *Biosensors* **2022**, *12*, 348.
60. W. Wu, L. Shi, Y. Duan, S. Xu, X. Gao, X. Zhu, B. Liu, *Chem. Mater.* **2021**, *33*, 5974–5980.
61. F. Hu, S. Xu, B. Liu, *Adv. Mater.* **2018**, *30*, 1801350.
62. Q. Wang, Q. Chen, G. Jiang, M. Xia, M. Wang, Y. Li, X. Ma, J. Wang, X. Gu, *Chin. Chem. Lett.* **2019**, *30*, 1965–1968.
63. C.-C. Chang, M.-C. Hsieh, J.-C. Lin, T.-C. Chang, *Biomaterials* **2012**, *33*, 897–906.
64. G. B. Bodedla, W.-Y. Wong, X. Zhu, *J. Mater. Chem. A* **2021**, *9*, 20645–20652.
65. G. B. Bodedla, G. Tang, J. Zhao, X. Zhu, *Sustain. Energy Fuels* **2020**, *4*, 2675–2679.
66. A. Rananaware, R. S. Bhosale, K. Ohkubo, H. Patil, L. A. Jones, S. L. Jackson, S. Fukuzumi, S. V. Bhosale, S. V. Bhosale, *J. Org. Chem.* **2015**, *80*, 3832–3840.
67. R. Wang, S. Chen, Q. Chen, H. Guo, F. Yang, *Dyes Pigm.* **2021**, *190*, 109332.
68. T. T. Tasso, T. Furuyama, J. Mack, T. Nyokong, N. Kobayashi, *Eur. J. Inorg. Chem.* **2015**, *2015*, 5516–5522.

How to cite this article: G. B. Bodedla, X. Zhu, W. Y. Wong, *Aggregate* **2023**, *4,* e330. https://doi.org/10.1002/agt2.330

AUTHOR BIOGRAPHIES

Dr. Govardhana Babu Bodedla obtained his M.Sc. degree from Acharya Nagarjuna University (ANU) in 2010 and a Ph.D. degree from the Indian Institute of Technology Roorkee (IITR) in 2016, India. From 2017 to 2020, he worked as a postdoctoral researcher (with Dr. Xunjin Zhu) at Hong Kong Baptist University. Since 2020, he has been working as a postdoctoral researcher (with Prof. Wai-Yeung Wong (Raymond)) at The Hong Kong Polytechnic University. His current research interests focus mainly on the rational design and synthesis of tetrapyrrolic macrocycle-based photocatalysts for sustainable green-energy technologies such as photocatalytic hydrogen evolution and conversion of carbon dioxide to value-added chemicals.

Dr. Xunjin Zhu obtained his Ph.D. degree in 2006 at the Department of Chemistry, Hong Kong Baptist University, and worked at the University of Texas at Austin and Georgia Institute of Technology as a postdoctoral fellow from 2006 to 2010. Dr. Zhu started his academic career as Research Assistant Professor in 2010, Assistant Professor in 2013, and Associate Professor in 2019 at the Department of Chemistry, Hong Kong Baptist University. His current research interests focus on the design and synthesis of porphyrin materials for various green technologies, ranging from organic solar cells, artificial photosynthesis, to electrocatalysis.

Professor Wai-Yeung Wong obtained his B.Sc.(Hons.) and Ph.D. degrees from the University of Hong Kong. After postdoctoral works at Texas A&M University (with Prof. F.A. Cotton) and the University of Cambridge (with Profs. Lord Lewis and P.R. Raithby), he joined Hong Kong Baptist University from 1998 to 2016 and now works at the Hong Kong Polytechnic University as the Dean of Faculty of Science and Chair Professor of Chemical Technology. Among his awards are the RSC Chemistry of the Transition Metals Award, FACS Distinguished Young Chemist Award, State Natural Science Award from China, and RGC Senior Research Fellow Award. His research focuses on synthetic inorganic/organometallic chemistry, aiming at developing photofunctional metal-organic molecules and polymers for optoelectronic and energy-related applications.